Investigating the superfluidic behaviour of photon Bose-Einstein condensates with thermo-optic non-linearities

Clara Bartels

Bachelorarbeit in Physik
angefertigt im Institut für Angewandte Physik

vorgelegt der
Mathematisch-Naturwissenschaftlichen Fakultät
der
Rheinischen Friedrich-Wilhelms-Universität
Bonn

Juli 2016

Ich versichere, dass ich diese Arbeit selbstständig verfasst und keine anderen als die angegebenen Quellen und Hilfsmittel benutzt sowie die Zitate kenntlich gemacht habe.

Bonn, ...
Datum Unterschrift

1. Gutachter: Prof. Dr. Martin Weitz
2. Gutachter: Dr. Frank Vewinger

Contents

1 Introduction **1**

2 Theory **3**
2.1 The Thermo-Optic Effect . . . 3
2.2 Discretization . . . 4
2.3 Normalization . . . 4

3 Steady State **7**
3.1 Green's function . . . 7
3.2 Implementation . . . 10
3.3 Results and Discussion . . . 11
3.4 Time Independent Perturbation Theory . . . 13

4 Dispersion **17**
4.1 The Landau Criterion of Superfluidity . . . 17
4.2 Two Different Cases . . . 17
4.3 Results and Discussion . . . 18

5 Time Dependent Problem **23**
5.1 Crank-Nicholson . . . 23
5.2 Excitation . . . 24
5.3 Eigenfrequencies . . . 24

6 Conclusions and Outlook **27**

A Appendix **31**

CHAPTER 1

Introduction

Bose-Einstein condensation occurs when the de-Broglie wavelength of bosons becomes larger than the average distance between particles. In this case, the ground state becomes macroscopically occupied and a new quantum state of matter can be observed. This was first predicted by Albert Einstein and Satyendra Nath Bose in 1924 [**1**] and experimentally achieved in 1995 by Eric Cornell and Carl Wieman in JILA [**2**], where Alkali atoms were cooled down to very low temperatures via laser and evaporative cooling. While photons are also bosons, they typically do not condense as the chemical potential vanishes. This results in a decrese in the photon number when the system is cooled down. To overcome this a process is needed in which temperature and photon number can be changed independently. This was achieved in 2010 by Jan Klaers, et. al. in Bonn [**3**] in a dye-solution filled microcavity. The separation of the mirrors, whose distance is in the micrometer regime, means that only photons with a certain minimal energy can exist between them. As the minimal energy given by the mirrors is much larger (2.1 eV) than the thermal energy (1/40 eV)[**4**], there is almost no purely thermal excitation of the photons. Repeated collisions between photons and dye molecules lead to a thermalization of the photon gas at room temperature [**4**]. The photons in the cavity have an effective mass of

$$m_{eff} = \hbar\omega\left(\frac{n_0}{c}\right)^2 \tag{1.1}$$

where ω is the cut-off frequency of the cavity and n_0 is the refractive index of the solvent. This mass is much smaller than that of an atom, which means that Bose Einstein condensation can be observed at room temperature instead of the extremely small temperatures needed for atomic BECs.
While superfluidic behaviour has been observed in BECs in cold atomic gases[**5**], it is yet unclear whether photon BEC also exhibits superfluidity. The photons colliding with the dye molecules change their temperature, and in turn their refractive index. This leads to an effective photon-photon interaction In this thesis I find ways to numerically solve the equations that arise when investigating the behaviour of the wave function and temperature of the system under the effect of thermo-optic non-linearity to see if its behaviour shows signs of superfluidity. In the first chapter I offer the theoretical foundations and the equations I aim to solve for the wave function and the temperature of the system. In the second chapter I look at the steady state behaviour of the system and at how the different parameters in the experimental setup can influence the condensate. I also use the time-independent perturbation theory to get an alternative solution for the values obtained in the previous chapter and compare them, as well as a theoretical understanding of the behaviour observed. In the fourth chapter I investigate the dispersion relation with regard to Laundau's criteria of superfluidity. Finally, I investigate the time-dependent behaviour of the system, investigating how the photon gas reacts to small perturbations and find the

eigenfrequencies. Chapter six gives a conclusion and an outlook on future investigations.
The equations I solved and the theoretical investigations were done by Dr. Hadiseh Alaeian, who supervised this thesis. MATLAB [**6**] was employed for computer programming and numerical analysis.

CHAPTER 2

Theory

2.1 The Thermo-Optic Effect

The interaction in the system is caused by the thermo-optic effect. A change of beam intensity leads to a heating of the system. This in turn changes the refractive index, similar to the Kerr effect, and changes the way in which other photons interact with it. This process results in repulsive or attractive photon-photon interaction. While repulsive in most gases or liquids, the interaction is attractive in solids. The wave equation in a non-linear medium is:

$$\nabla^2 E - \frac{n_0^2}{c^2}\frac{\partial^2 E}{\partial t^2} = \frac{1}{\epsilon_0 c^2}\frac{\partial^2}{\partial t^2}P^{NL} \tag{2.1}$$

With $P = \epsilon_0\left(\chi^{(L)} + \chi^{(NL)}\right)$ and $\chi^{(NL)} = 2n_0\frac{dn}{d\Delta T}\Delta T$ one can write (2.1) as

$$\nabla^2 E - \frac{n^2}{c^2}\frac{\partial^2 E}{\partial t^2} = \frac{2n_0}{c^2}\frac{dn}{d\Delta T}\frac{\partial^2 \Delta T E}{\partial t^2} \tag{2.2}$$

For the electric field one can assume:

$$E(x, y, z, t) = \Psi(x, y, z, t)e^{-i\omega t} \tag{2.3}$$

The envelope is slowly varying, meaning that the term with $\ddot{\Psi}$ can be dropped. After plugging this back into (2.2) and following some manipulations (2.2) becomes:

$$i\dot{\Psi} = -\frac{\omega}{2}\Psi - \frac{1}{2\omega}\left(\frac{c}{n_0}\right)^2\nabla^2\psi - \frac{\omega}{n_0}\left(\frac{dn}{d\Delta T}\right)T\Psi \tag{2.4}$$

The change of the temperature is given by the heat equation:

$$\frac{\partial \Delta T}{\partial t} = \frac{\kappa}{C_v}\nabla^2\Delta T + \frac{\alpha n_0}{2C_v Z_0}|\Psi|^2 \tag{2.5}$$

(2.4) and (2.5) now give a set of coupled equations that need to be solved in order to obtain the form of the wave function Ψ and the temperature T. Note that for simplicity from now on instead of ΔT I write T , referring to the difference in temperature with respect to room temperature, not the absolute temperature.

Also for simplicity the following coefficient are introduced:

$$A = -\frac{\omega}{2} \tag{2.6}$$

$$B = -\frac{1}{2\omega}\left(\frac{c}{n_0}\right)^2 \tag{2.7}$$

$$C = -\frac{\omega}{n_0}\left(\frac{dn}{d\Delta t}\right) \tag{2.8}$$

$$D = \frac{\kappa}{C_v} \tag{2.9}$$

$$E = \frac{\alpha n_0}{2T_0 C_v Z_0} \tag{2.10}$$

The parameters that I used are given in Table 2.1 and should correspond to those of the experiment. L is the length of the cavity. Note that while the mirrors are curved in reality, the curvature is so small that for the sake of simplicity I assumed plane mirrors. α is the absorption of the system, C_v the volumetric heat capacity and n_0 the refractive index.

Table 2.1: the experimental parameters I used in my calculation. L and α were varied in some cases.

n_0	L (μm)	$\frac{dn}{dT}(K^{-1})$	$C_v(JK^{-1}cm^{-3})$	$\alpha(m^{-1})$	$\kappa(Wm^{-1}K^{-1})$	$Z_0(\Omega)$
1.33	2	-4.8×10^{-4}	1.9	0.059	0.168	376, 73

2.2 Discretization

I solved the coupled equations given above by discretizing in space and time. I used polar coordinates where the z-axis is the longitudinal direction between the two mirrors, with the origin being in the middle of the cavity, so that z is defined between $-L/2$ and $L/2$ (see Figure 2.1). Depending on the longitudinal mode number q I used 20 to 75 discrete points. In reality, there is a quadratic trapping potential in the transverse direction. It was dropped here, meaning that in theory the radial direction should be considered up into infinity. In my discretization, the radial direction ρ was defined from 0 to $R_{max} = 5L$, which turned out to be a sufficiently large space for the wave function to tail off by itself and fulfil the boundary condition of being zero at $\rho = R_{max}$. To keep $\Delta\rho$ and Δz similar, the number of points in this direction was five times that of the z-direction. This led to very big arrays, especially for the higher mode numbers where greater accuracy in the z-direction was needed, which limited the calculations I could carry out.

2.3 Normalization

One problem I encountered is the large discrepancy in the order of magnitude of the parameters, which can lead to numerical complications. In an effort to make the calculations more manageable, I found normalized versions of the coefficients. For this I introduced the normalization parameters a, τ, E_0 and

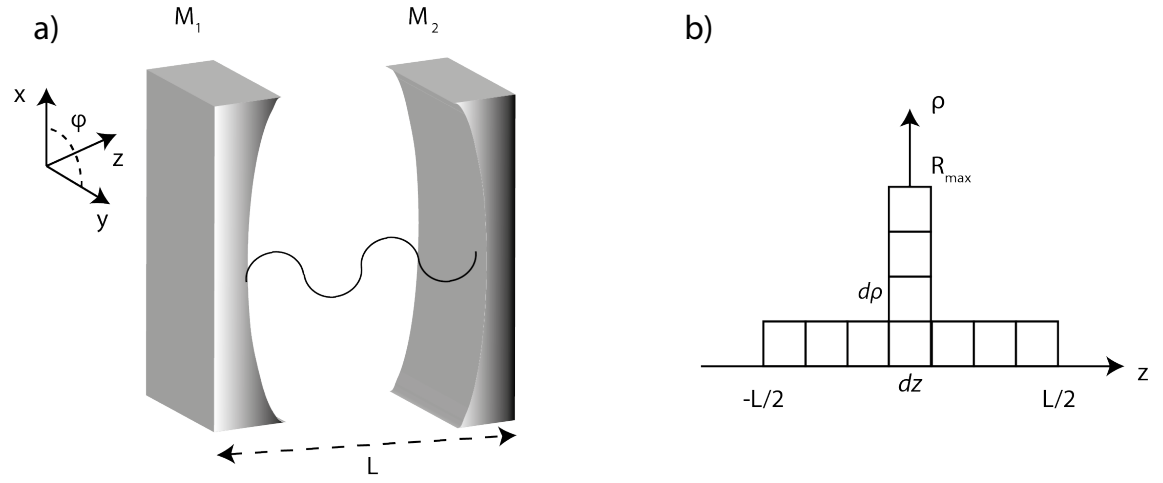

Figure 2.1: A schematic of the cavity and the discretization that was used.Figure a) shows the curved mirrors of the cavity with the cavity length L. The curvature is very small, which is why for my calculations I assumed plane mirrors. Figure b) shows the discretization that was used in the z- and ρ-direction. The origin of the coordinate system I used is at the centre of the cavity.

T_0:

$$L \to aL'$$
$$t \to \frac{t'}{tau}$$
$$\Psi \to E_0\Psi'$$
$$T \to T_0T'$$

The normalized version of the coupled equations is:

$$i\dot{\Psi} = \mathcal{A}\Psi + \mathcal{B}\nabla^2\Psi + \mathcal{C}T\Psi \tag{2.11}$$
$$\dot{T} = \mathcal{D}\nabla^2T + \mathcal{E}|\Psi|^2 \tag{2.12}$$

with new parameters

$$\mathcal{A} = -\frac{\omega\tau}{2} \tag{2.13}$$
$$\mathcal{B} = -\frac{\tau}{2\omega}\left(\frac{c}{n_0}\right)^2\frac{1}{a^2} \tag{2.14}$$
$$\mathcal{C} = -\frac{\omega\tau}{n_0}\left(\frac{dn}{d\Delta t}\right)T_0 \tag{2.15}$$
$$\mathcal{D} = \frac{\kappa\tau}{C_v}\frac{1}{a^2} \tag{2.16}$$
$$\mathcal{E} = \frac{\alpha n_0\tau}{2T_0C_vZ_0}|E_0|^2 \tag{2.17}$$

I chose τ to be $\frac{1}{\omega}$ and a so that $\mathcal{B}$ would be -0.5 in agreement with many other equations in the literature. E_0 was chosen so that the wave function is properly normalized and T_0 set such that $\mathcal{E} = \mathcal{D}$.

CHAPTER 3

Steady State

First, I looked at the system once it has reached the steady state Here, $\dot{T}$ has become zero and the wave function only varies harmonically. For the wave function, one can assume the form of $\Psi(r)e^{-i\mu t}$. μ is a frequency, which corresponds to the chemical potential via multiplication by $\hbar$. Notice that the time dependence in Ψ has been dropped. In the steady state, the coupled equations thus simplify to:

$$i\mu\Psi_{ss} = A\Psi_{ss} + B\nabla^2\Psi_{ss} + CT\Psi_{ss} \tag{3.1}$$

$$0 = D\nabla^2 T_{ss} + E|\Psi_{ss}|^2 \tag{3.2}$$

3.1 Green's function

To find the temperature T_{ss}, one first needs to solve the Green's function:

$$T_{ss}(x,y,z) = -\frac{E}{D}\int_{V_c} G(x,y,z;x',y',z')|\psi_{ss}(x',y',z')|^2 dr' \tag{3.3}$$

$$\nabla^2 G(\vec{r};\vec{r}') = \delta(\vec{r}-\vec{r}') \tag{3.4}$$

The boundary conditions state that T and Ψ are zero at the mirrors, for $z = \pm L/2$:

$$G(z = \pm L/2) = 0 \tag{3.5}$$

Using the mirror imaging technique one gets the following series expansion:

$$G_1(\vec{r};\vec{r}') = -\frac{1}{4\pi}\sum_{n=-\infty}^{+\infty}\left(\frac{1}{\sqrt{\rho^2+(z-z'+2nL)^2}} - \frac{1}{\sqrt{\rho^2+(z+z'+(2n+1)L)^2}}\right) \tag{3.6}$$

with $\rho^2 = (x-x')^2 + (y-y')^2$.

The above form, however, only converges well for cases in which $\rho \leq L$, i.e. close to (x', y', z'). For

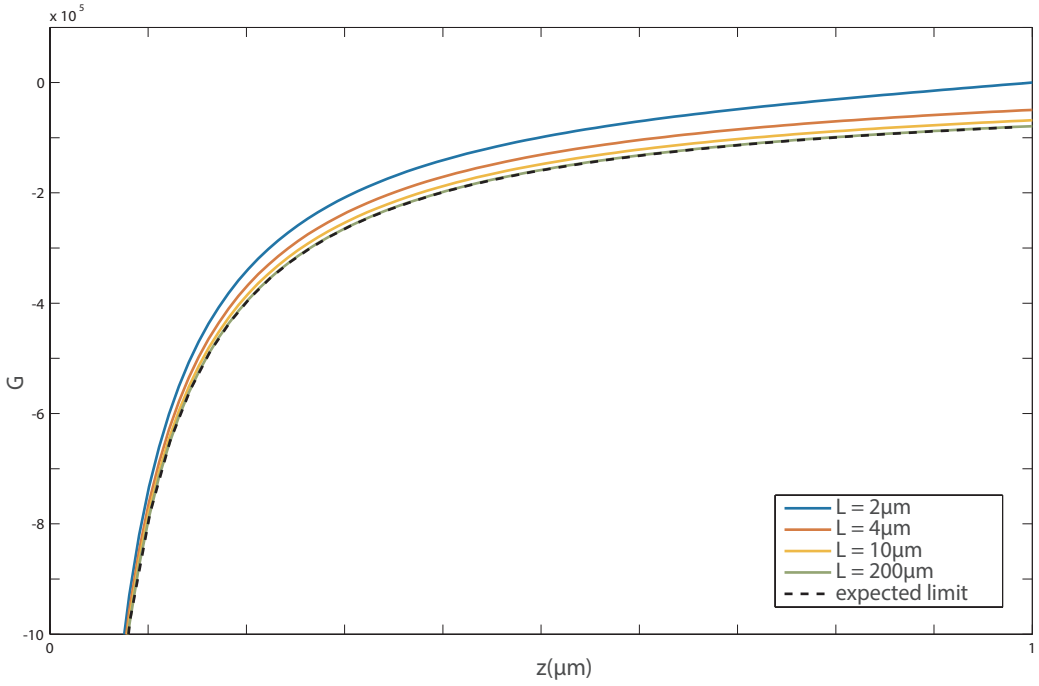

Figure 3.1: The Green's function as a function of z at $\rho = 0$, $z' = 0$ for different cavity lengths L. It can be seen that for large values of L, the Green's function converges to the theoretically expected limit of $\frac{1}{4\pi z}$, as every term including L becomes too small to play a role. For the length scales given in the experimental set-up, the cavity length still controls the non-locality.

cases with greater ρ there is another series with better convergence:

$$G_2(\vec{\rho}, z; \vec{\rho}', z') = -\frac{1}{\pi L} \sum_{n=1}^{M} sin\left(\frac{n\pi}{L} z\right) sin\left(\frac{n\pi}{L} z'\right) K_0\left(\frac{n\pi}{L} |\vec{\rho} - \vec{\rho}'|\right) \tag{3.7}$$

I calculated the Green's function via both formulas for a number of $\vec{r}, \vec{r'}$ and found out while they gave very similar results, as expected the first version needed a rapidly increasingly number of terms to converge for larger ρ. (see Table 3.1)

At $\vec{\rho} = \vec{\rho'}$, the Green's function becomes singular. However, as I have to integrate over the full space, I have to overcome this. As it turns out, Matlab is able to integrate over the singularity, but it takes quite some time doing so. Since the discretization results in a large matrix, this would result in a very long run time. To circumvent this, I looked at replacing the integration with a summation over very small cubes. To test accuracy and speed of the different methods, I compared three different methods of integration (using `triplequad`, `integral3` and `integral`) and the summation for points outside the singularity. Parts of the results are shown in Table 3.2. It turned out that `quad` is the fastest and most stable method out of the three, and so I decided to use that for further calculations. Next, I tested the results for the singularity itself, using Mathematica as an extra test for the accuracy. [1] While the summation is much faster than `quad`, it also becomes very inaccurate at the singularity itself, which is why I decided to keep using `quad` for the singular terms.

[1] Mathematica is able to do it, but takes a very long time. I did not want to keep switching between programmes and consequently decided against using it.

Table 3.1: The different summations for the Green's function for $z = z' = 0$ and different values for $\frac{\rho}{L}$. N is the number of terms needed for the sum to converge. One can see that for large ρ, the first summation quickly becomes very slow.

$\frac{\rho}{L}$	G_1	N	G_2	N
0	-	-	-	-
1.0526	-0.006	113	-0.006	100
2.1053	-1.5353E-04	386	-1.5350E-04	100
3.1579	-4.6153E-06	1241	-4.6125E-06	100
4.2105	-1.4702E-07	3917	-1.4673E-07	100
5.2632	-4.8453E-09	12220	-4.8157E-09	100
6.3158	-1.6432E-10	37715	-1.6121E-10	100
7.3684	-5.8375E-12	109919	-5.4716E-12	100
8.4211	-2.6790E-13	234617	-1.8759E-13	100
9.4737	-7.0562E-14	262665	-6.4814E-15	100

Table 3.2: Comparing the different integration/summation methods for the Green function and the corresponding computation times. $L = 1$, $R_{max} = 10$, $N_r = 15$, $N_z = 5$, $z = z' = -0.25$, $\phi = 0$ $r' = \Delta r$

$r/\Delta r$	Summation	time/s	`quad`	time/s	`integral3`	time/s	`integral`	time/s
2	-0.0030	0.01856	-0.0031	2.277	-	-	-0.0027	240.554
3	-2.3977E-04	0.02963	-2.3752E-04	1.775	-2.3739E-04	10.324	-2.3870E-04	227.365
4	-2.3023E-05	0.01213	-2.2742E-05	1.208	-2.2695E-05	9.338	-2.3051E-05	225.273
5	-2.3164E-06	0.02835	-2.3002E-06	1.220	-2.2958E-06	6.684	-2.3267E-06	226.810
6	-2.3943E-07	0.02098	-2.3879E-07	1.199	-2.3836E-07	4.659	-2.4099E-07	229.130
7	-2.5190E-08	0.02740	-2.5200E-08	1.207	-2.5156E-08	2.961	-2.5390E-08	227.234
8	-2.6834E-09	0.02964	-2.6905E-09	1.208	-2.6859E-09	2.358	-2.7075E-09	225.358
9	-2.8851E-10	0.02355	-2.8977E-10	1.219	-2.8927E-10	1.469	-2.9133E-10	225.029
10	-3.1244E-11	0.00817	-3.1422E-11	1.211	-3.1369E-11	1.398	-3.1568E-11	224.191
11	-3.4028E-12	0.02461	-3.4259E-12	1.224	-3.4203E-12	1.393	-3.4399E-12	224.150
12	-3.7233E-13	0.02998	-3.7519E-13	1.219	-3.7459E-13	1.375	-3.7655E-13	224.909
13	-4.0899E-14	0.02770	-4.1244E-14	1.216	-4.1179E-14	1.383	-4.1376E-14	224.042
14	-4.5072E-15	0.02975	-4.5481E-15	1.212	-4.5411E-15	1.386	-4.5612E-15	223.743
15	-4.9811E-16	0.02575	-5.0290E-16	1.208	-5.0214E-16	1.389	-5.0420E-16	224.626

Later, I tried to find a more accurate approximation for the singular term in the summation by changing the form of the volume from a cube to a cylindrical cell. While being closer to the exact value, it is still not very plausible. In the end I settled on a mixture of the two methods, using the `quad` integration for the singular terms while calculating the other terms via the summation to get an acceptable compromise of speed and accuracy.
Another way I tried later was calculating the inverse of the Laplacian without finding the closed form of the Green's function at all.

$$T_{ss} = -\frac{E}{D}\left(\nabla^2\right)^{-1} |\Psi_{ss}(x', y', z')|^2 \tag{3.8}$$

Comparing the results to the former method, they seemed accurate, and much faster to compute because there was no need to calculate the matrix of the Green's function beforehand. This is the method I used

for all the final results presented in this thesis.

3.2 Implementation

The steady state solution is computed using an iterative method. Via the Green's function or the inverse Laplacian I find the temperature corresponding to the initial wave function and then use that value to compute the next iteration of the wave function. This presents an eigenvalue problem which Matlab can solve via the `eig` function, where the wave function is given by the eigenvector and the eigenvalue represents the frequency μ. To get a rough idea of what to expect, I solved the equation for the wave function (3.1) without the non-linearity (meaning $C = 0$) using separation of variables. The problem has rotational symmetry in the ϕ-direction and a sinusoidal behaviour along the z-axis, leaving only the ρ-direction to be determined. I get a Bessel function for that part, which leads to the following solution for the linear wave function:

$$\Psi_{lin}(\rho, z, \phi) = R(\rho)Z(z)\Phi(\phi) = A_N J_N(k_\rho, \rho) sin\left(\frac{q\pi}{L}\left(z + \frac{L}{2}\right)\right) e^{.iN\phi} \tag{3.9}$$

where $A_N = \sqrt{\frac{2N_{BEC}}{\pi L R_{max}^2 J_{N+1}^2(k_\rho, Rmax)}}$ is the normalization factor chosen to satisfy the normalization condition of $\int |\Psi|^2 dV = N_{BEC}$, q is the longitudinal mode number, N_{BEC} the number of photons in the condensate and k_ρ is given by

$$k_\rho = -\left(\frac{\mu - A}{B}\right) - \left(\frac{q\pi}{L}\right)^2 \tag{3.10}$$

Here, μ can be determined via (3.9) and the boundary conditions $\Psi(\rho = R_{max}) = 0$:

$$\mu_{lin} = -B\sqrt{\left(\frac{b}{R_{max}}\right)^2 + \left(\frac{q\pi}{L}\right)^2} \tag{3.11}$$

where b is the first zero of the Bessel function J_N.
The temperature is dependent only on $|\Psi(\rho, z)e^{-iN\phi}|^2$, and thus independent of ϕ. This can easily be seen when looking at the Fourier series and plugging it in (3.2):

$$T(\rho, \phi, z) = \sum_n T_n(\rho, z) e^{in\phi} \tag{3.12}$$

$$\nabla^2 T = -\frac{E}{D} \sum_n \left(\nabla_\rho^2 - \frac{n^2}{\phi^2} + \nabla_z^2\right) T_n(\rho, z) e^{in\phi} = -\frac{E}{D} |\Psi_s s(\rho, z)|^2 \tag{3.13}$$

As the RHS is independent of ϕ, the only viable solution for (3.13) is $n = 0$.

I used (3.9) as the starting wave function for Ψ to iteratively calculate the steady state solution, and found that it converges after a three or four steps. As (3.1) is an eigenvalue problem, for each step there are several solutions for the eigenvalue μ to choose from. To decide which one to use I looked at the analytical solution for μ in the linear case, (3.11), and used it as a reference. The original idea was to choose the eigenvalue that was closest to this but higher, as one expects a positive change. However, testing revealed that this μ did not always yield proper results, as the corresponding wave functions showed ripples that were not physical but instead due to the numerical discretization. Thus, it was necessary to choose each eigenvalue by individually checking the wave functions it gave. To do this, I

solved the linear case numerically, which, when solved correctly, should simply return the original wave function, and then looked for the eigenvalue which showed that wave function. This $\mu_{start,num}$ was then used as a reference for calculating $\Delta\mu$ for the non-linear case. In Figure 3.2 an example of the distribution of the eigenvalues is shown.

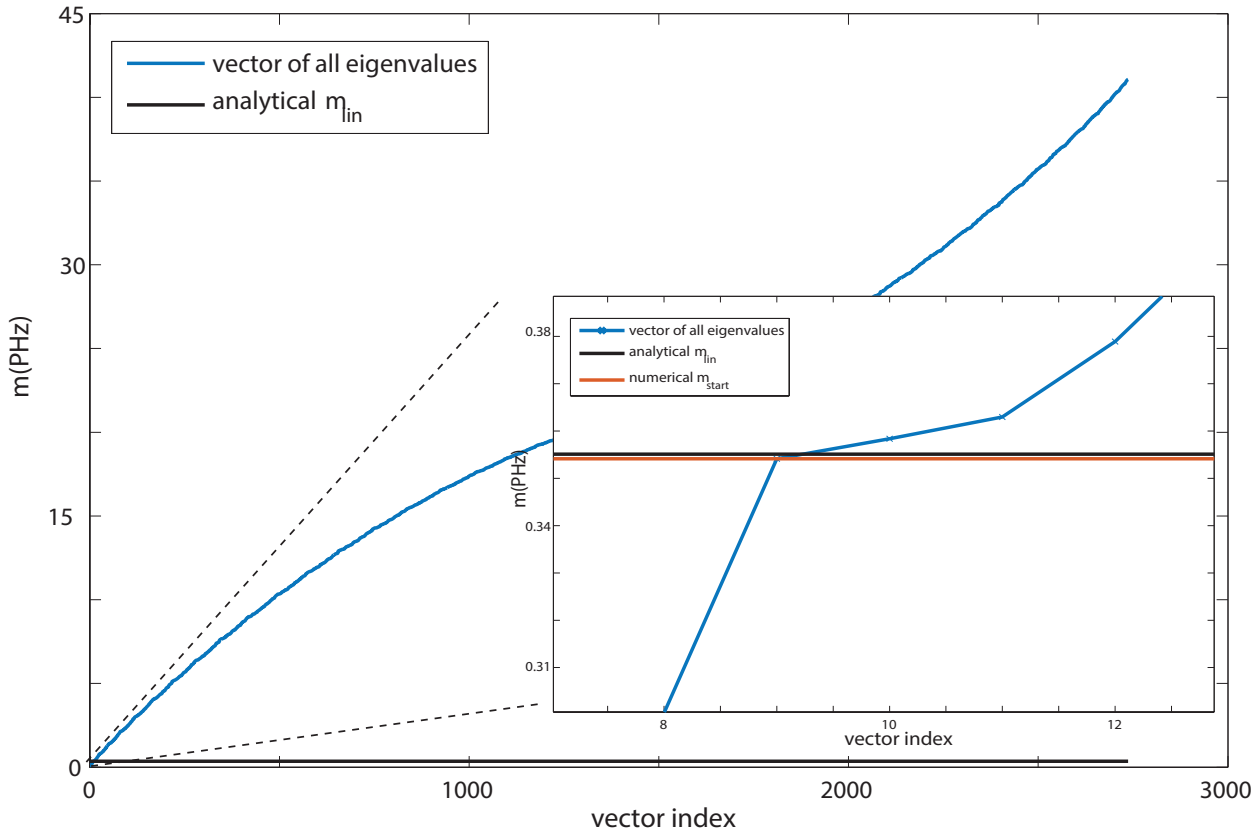

Figure 3.2: A graphical representation of all the different eigenvalues the numerical solution gives (blue). Black is μ_{lin} that was analytically calculated for the linear case. One can clearly see that the vast majority of eigenvalues can be immediately discarded as they are too large. The inset shows a closer look at the eigenvalues in the actual region of interest. The red line here is the eigenvalue that corresponds to the wave function with the proper shape and which was used as a reference to find $\Delta\mu$ in the non-linear case. The μ found for this case are between both lines, which is why using μ_{lin} as a reference would yield negative values for $\Delta\mu$

3.3 Results and Discussion

I computed the steady state solution for different values of angular momentum (N) and longitudinal mode number (q). For each case, a set of different values for photon number (N_{BEC}) and absorption (α) was used. As expected, the temperature scaled linearly with both N_{BEC} and α (see Figure 3.5). This is to be expected, as E, the coefficient in front of the temperature in 3.1, is linearly proportional to α, while the normalization coefficient in front of Ψ is proportional to $\sqrt{N_{BEC}}$, and T is also proportional to $|\Psi|^2$. Figures 3.3 and 3.4 show the shape of wave function and temperature for $q = 1$ and $N = 0$ or $N = 1$,

respectively. Comparing the two, one can clearly see a shift of the maximum away from the center of the cavity. In the appendix, one can also see the case for $q = 7$.
For better overview, I plotted both the change in frequency - proportional to the chemical potential - $\Delta\mu$, and $\langle\rho\rangle$, the expectation value of ρ in the wave function, which should give an indication about the radius of the BEC. Figure 3.6 shows that the non-locality increases with both N_{BEC} and α. The behaviour for different q and N can also be seen (see Figures A1 and A2): $\Delta\mu$ and $\langle\rho\rangle$ increase with both N and q.

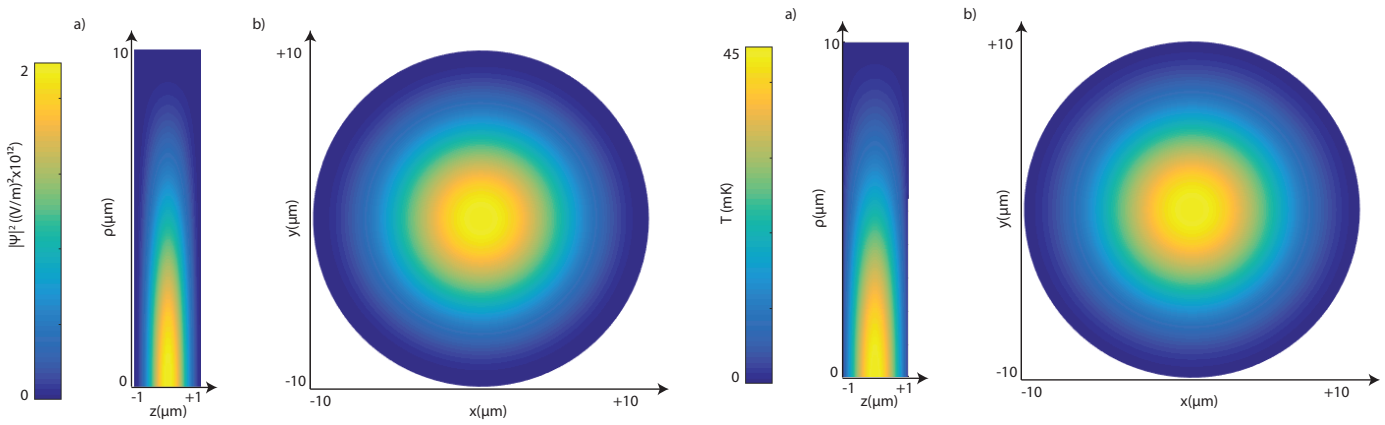

Figure 3.3: This figure shows the intensity of the wave function $|\Psi|^2$ (left) and the temperature T (right) both in the $\rho - z$-direction (a) and the $x - y$-plane (b) for $q = 1$ and no angular momentum. One can see that the maximum in both cases is centred around the middle of the cavity. The parameters were: $N = 0$, $q = 1$, $N_{BEC} = 40000$ and $\alpha = 0.059\,\mathrm{m}^{-1}$

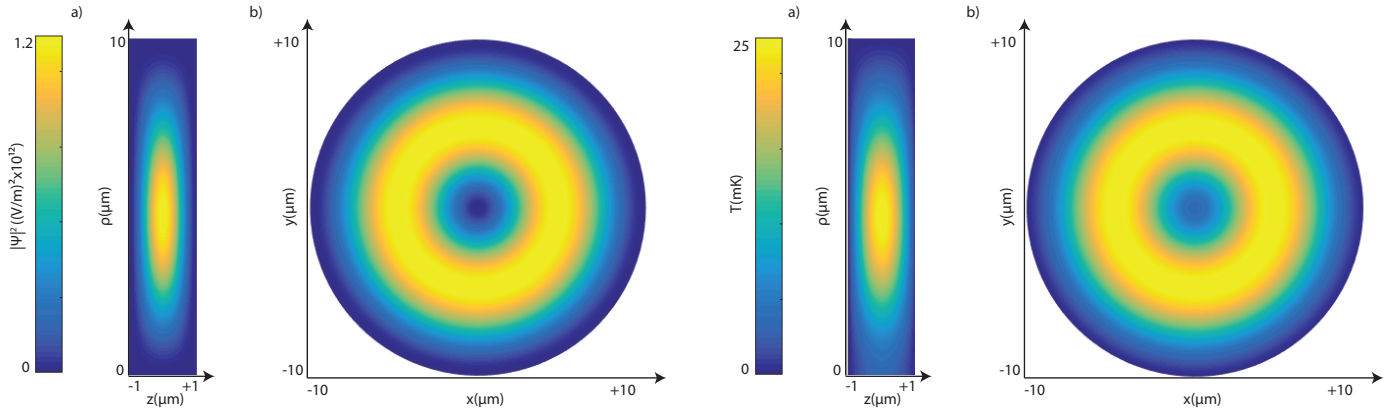

Figure 3.4: This is similar to Figure 3.3, except that here there is an angular momentum $N = 1$. In contrast to Figure 3.3 the maximum has now moved away from the centre. This is in agreement with the behaviour observed for $\langle\rho\rangle$, which increases with larger N (see Figure A1). The parameters were: $N = 1$, $q = 1$, $N_{BEC} = 40000$ and $\alpha = 0.059\,\mathrm{m}^{-1}$

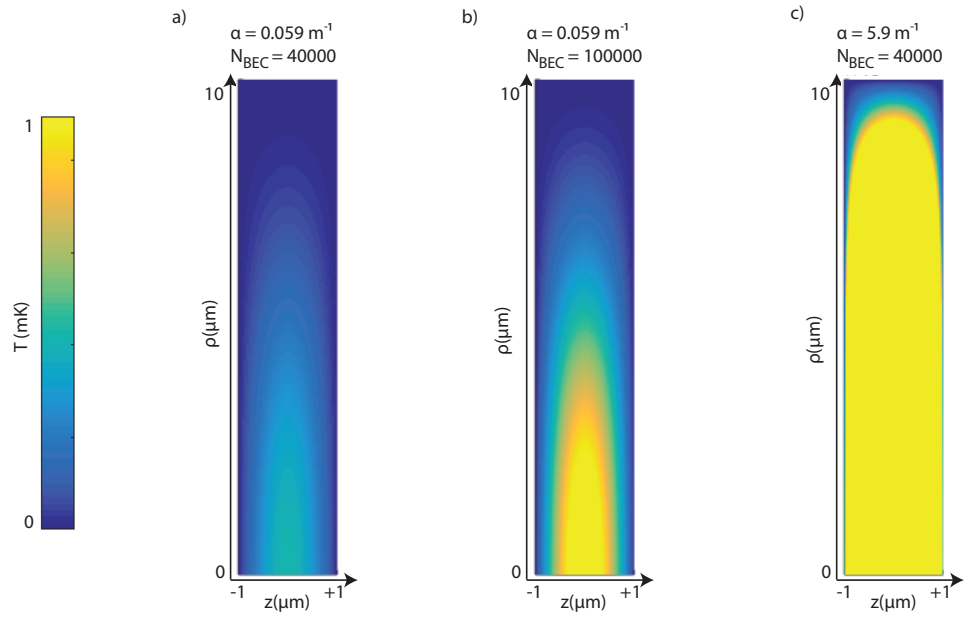

Figure 3.5: This shows the temperature in the $\rho - z-$plane for different values of α and N_{BEC}. Between (a) and (b) the number of photons was increased, while (c) has an interaction coefficient 100 times larger than (a). In both cases, the temperature increases. Here, $q = 1$ and $N = 0$ was used.

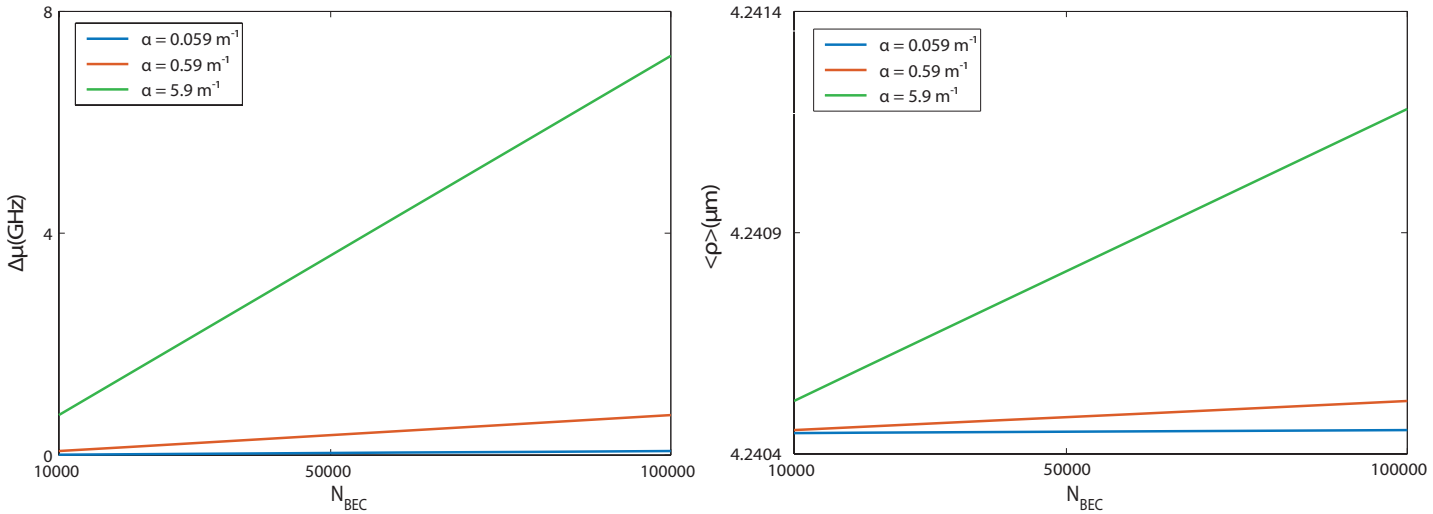

Figure 3.6: The change in frequency $\Delta\mu$ as well as the expectation value of ρ for the wave function in the case of $N = 0$ and $q = 1$ as a function of N_{BEC} α. While the changes in $\langle\rho\rangle$ are very small, one can still see a rise in non-locality with both increasing N_{BEC} and α.

3.4 Time Independent Perturbation Theory

To understand the results better, I looked at an alternative way to calculate the effect of the non-linearity. In the steady state solution, the perturbation of the wave function comes from the CT_{ss}-term only. Using

perturbation theory, this can be expressed by

$$\Delta\mu = \frac{\langle\Psi_{lin}| - C\frac{E}{D}\int dr' G(r,r)|\Psi_{un}|^2|\Psi_{lin}\rangle}{\langle\Psi_{lin}|\Psi_{lin}\rangle} \tag{3.14}$$

with Ψ_{lin} given by (3.9) and G the Green's function as given by (3.7). For the case of $N = 0$ this gives

$$\Delta\mu = C\frac{E}{D}\frac{1}{\pi L}\frac{|A_N|^4}{\langle\Psi_{lin}|\Psi_{lin}\rangle}\sum_{n=1}\left(\frac{4q^2((-1)^n-1)L}{2n\pi(n^2-4q^2)}\right)^2 \tag{3.15}$$

with the normalization factors

$$|A_N|^2 = \frac{4\hbar\omega}{\epsilon_0^2}\frac{N_{BEC}}{\pi R^2 L J_{N-1}^2(k_\rho R_{max})} \tag{3.16}$$

$$\langle\Psi_{lin}|\Psi_{lin}\rangle = \frac{2\hbar\omega N_{BEC}}{\epsilon_0 n_0^2} \tag{3.17}$$

As E is linearly proportional to α, that $\Delta\mu$ is also linearly proportional to α, as well as N_{BEC}. This behaviour was also observed in the previous calculations. Figure 3.7 shows the results obtained by this calculation for two different α. When comparing to the results of the steady state solution found previously one can see that while $\Delta\mu$ exhibits the same behaviour in regard to N_{BEC} and α, the results obtained via perturbation theory are higher by a factor of about 3 or 4. Figure 3.7 shows a comparison of the two methods, where I plotted $Delta\mu$ as a function of N_{BEC} for two different values of α. This discrepancy likely stems from the fact that while I only considered a bounded region up to a finite R_{max} in the numerical calculation, here the function is integrated over the whole space in the transverse direction. Despite this discrepancy, the agreement on the overall behaviour is encouraging, and it gives a physical explanation for the behaviour previously observed.

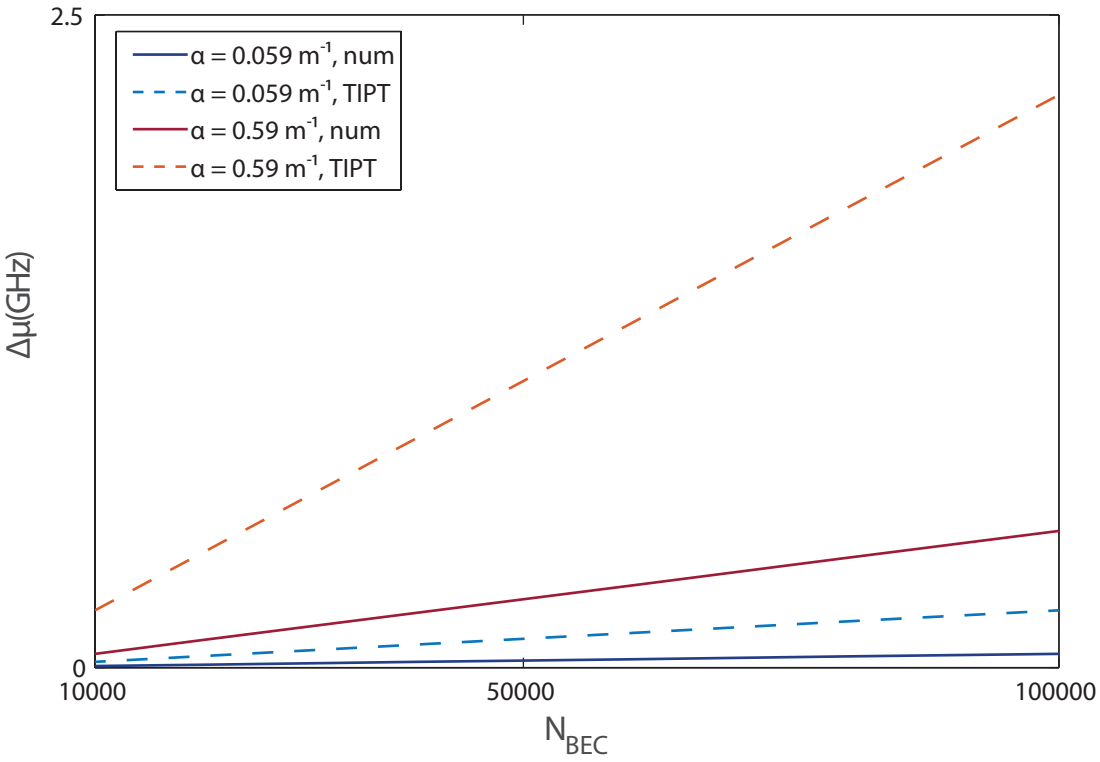

Figure 3.7: $\Delta\mu$ as a function of N_{BEC} for two different values of α, both numerically calculated from the steady state solution (num) and via the time independent perturbation theory (TIPT). The overall behaviour is similar, but the TIPT results are significantly higher than the numerical ones. This is probably due to the fact that while I used a closed region in the numerical solution, I integrated over the whole space for the perturbation theory calculations.

CHAPTER 4

Dispersion

4.1 The Landau Criterion of Superfluidity

One indication of superfluidic behaviour is the Landau criterion[**8**, **9**]. If an object with $\vec{p}_0 = M\vec{v}$ and a kinetic energy of $E_0 = \frac{1}{2}M\vec{v}^2$ moves through a fluid it can generate quasi-particles. This gives the new coupled equations for the object and the quasi-particle:

$$\vec{p} = M\vec{v} + \vec{k} \tag{4.1}$$

$$E = \frac{1}{2}Mv^2 + E(\vec{k}) + \vec{k} \cdot \vec{v} \tag{4.2}$$

where $\vec{k}$ is the momentum of the quasi-particle and $E(k)$ is the corresponding energy. The generation of quasi-particles only happens when it is energetically favourable, meaning that $\Delta E = E - E0 = E(\vec{k}) + \vec{k} \cdot \vec{v} < 0$. The energy of the quasi-particle is always positive, meaning that $\vec{k} \cdot \vec{v}$ has to be negative, i.e. the object and the quasi-particle are moving in opposite directions. From that one gets the following condition for the velocity:

$$v > \frac{E(k)}{k} \tag{4.3}$$

As one expects a non-zero critical velocity, this means that $E(\vec{k})$, and subsequently the dispersion, must be linear, similar to the sound velocity:

$$v_c = \lim_{k \to 0} \frac{E(k)}{k} \tag{4.4}$$

If this condition is met, one can reasonably assume that superfluidity is possible. However, it is not sufficient for superfluidity, but merely an indication.

4.2 Two Different Cases

The solution from the previous chapter can now be used to calculate the dispersion of the system. To investigate the dispersion, I looked at small variations around the steady state in the form of $e^{i\vec{k}\cdot\vec{\rho}}e^{i\omega t}$. There are two cases of interest that will be investigated separately:

a) non-local instantaneous interaction:

Here, the explicit time-dependency of the temperature is ignored, leading to the following equations:

$$i\dot{\Psi} = A\Psi + B\nabla^2\Psi + CT\Psi \tag{4.5}$$

$$0 = D\nabla^2 T + E|\Psi|^2 \tag{4.6}$$

The only interaction between the wave function and the temperature is now given by the Greens function which is independent of time, as it was in the steady state case. The dispersion relation is given by:

$$\omega^2 = B^2k^4 + 2\frac{BCE}{D}k^2|\Psi_{ss}(0)|^2\hat{G}(k) \tag{4.7}$$

$\hat{G}$ here is the Fourier transform of the Greens function, which is calculated via the Hankel transform and given by:

$$\hat{G} = -\frac{2}{L}\sum_n \left(\frac{4q^2((-1)^n - 1)}{n\pi(n^2 - 4q^2)}\right)^2 H_0(K_0\left(\frac{n\pi}{L}|\rho|\right) \tag{4.8}$$

$$H_0(K_0\left(\frac{n\pi}{L}|\rho|\right) = \left(\frac{L}{n\pi}\right)^2 \frac{1}{1 + \left(\frac{L}{n\pi}\right)^2 k^2} \tag{4.9}$$

b) non-local and delayed interaction:

For the more complete case, the Green's function is also dependent on the time. The dispersion relation becomes:

$$\omega^2 = B^2k^4 + 2\frac{BCE}{D}k^2|\Psi_{ss}(0)|^2\hat{G}(k,\omega) \tag{4.10}$$

with

$$\hat{G}(k,\omega) = -\frac{2}{L}\left(\frac{4q^2((-1)^n - 1)}{n\pi(n^2 - 4q^2)}\right)^2 H_0(k,\omega) \tag{4.11}$$

$$H_0(k,\omega) = \left(\frac{1}{\sqrt{\left(\frac{n\pi}{L}\right)^2 - i\omega}}\right)^2 \frac{1}{1 + k^2\left(\frac{1}{\sqrt{\left(\frac{n\pi}{L}\right)^2 - i\omega}}\right)^2} \tag{4.12}$$

Note that now the equation is implicit, meaning a minimization algorithm is needed to find the dispersion. This was done using the `fminsearch` function in Matlab, and proved relatively stable with regard to the starting guess. The solution now becomes complex, which corresponds to losses.

4.3 Results and Discussion

I plotted the dispersion relation for different parameters of q, N, α, N_{BEC}, and L, while keeping longitudinal mode number fixed at $q = 7$, which is the case of the actual experimental setup. For large momentum, $\omega(k)$ exhibits quadratic free particle behaviour. In the low momentum region a linear behaviour is observed. Two examples are shown in this section: Figure 4.1 shows the dispersion relation for the

non-local case for different α, and Figure 4.2 shows the non-local and delayed case for varying N_{BEC}. Further graphs are shown in the appendix.

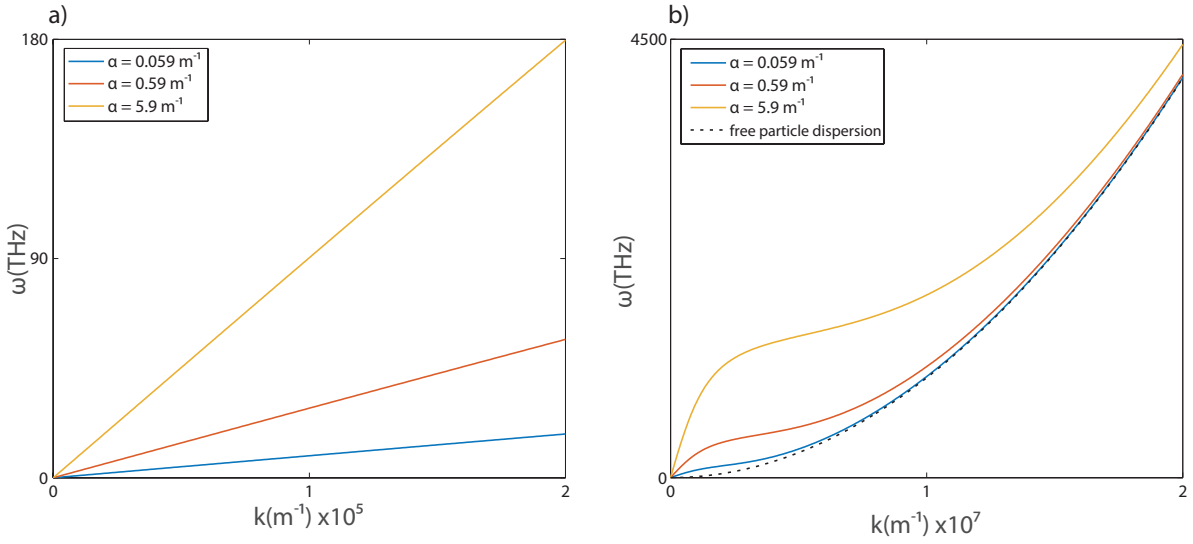

Figure 4.1: The dispersion relation for the non-local case for different values of α. The length of the cavity is $L = 2\,\mu m$ and the number of photons is $N_{BEC} = 40000$. Figure a) shows the low-momentum part with the linear behaviour, while b) is more zoomed out, showing the change towards quadratic behaviour. The dotted line correponds to the free particle behaviour, Bk^2.

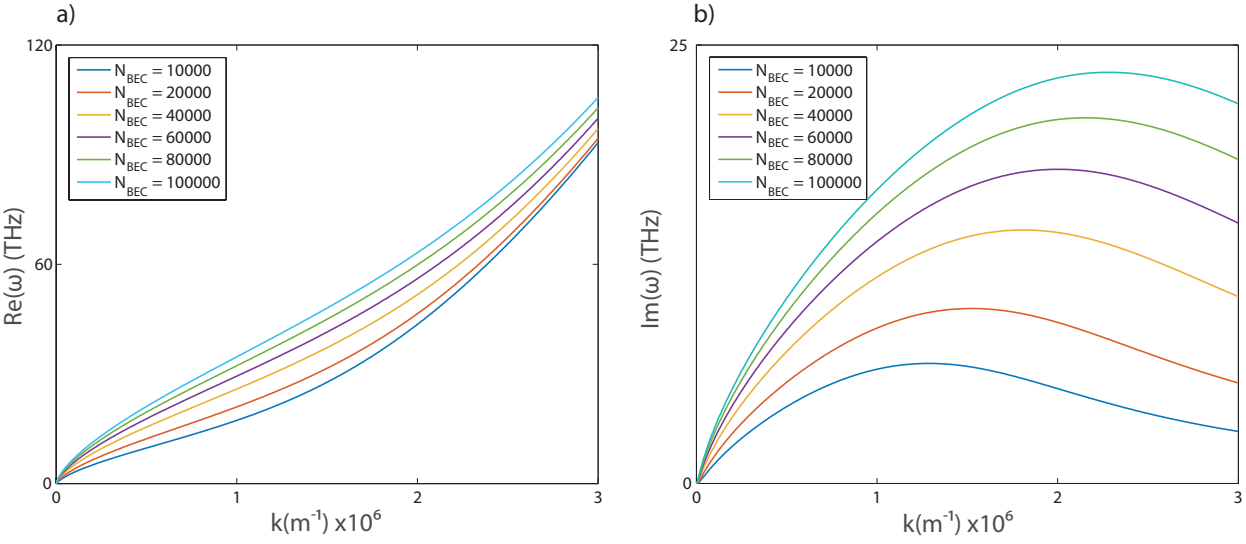

Figure 4.2: The dispersion relation for the delayed case for different values of N_{BEC}. The length of the cavity is $L = 2\,\mu m$ and the absorption is $\alpha = 0.059$. N_{BEC} was varied between 10^4 and 10^5. Figure a) shows the real part of the frequency, while b) shows the imaginary part, i.e. the losses. Both the linear region and the losses increase with N_{BEC}

The critical momentum k_{crit}, above which the free particle behaviour is dominant, is found by solving:

$$0 = \sqrt{2\frac{CE}{BD}|\Psi_{ss}|^2\hat{G}(k_{crit})} - k_{crit} \qquad \text{(non-local)} \tag{4.13}$$

$$0 = \omega^2 - B^2k^4 + 2\frac{BCE}{D}|\Psi_{ss}|^2k^2\hat{G}(k_{crit},\omega) \qquad \text{(non-local and delayed)} \tag{4.14}$$

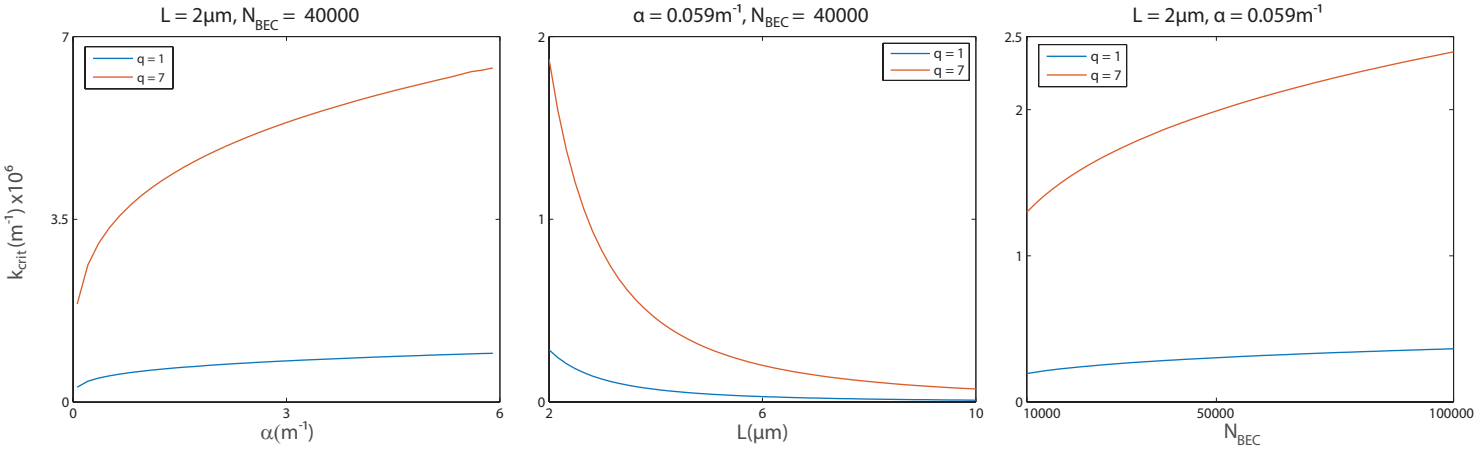

Figure 4.3: The behaviour of k_{crit} for the case of non-local and delayed interaction when varying different parameters for different mode numbers q. The fixed parameters were: $N = 0$, $L = 2\,\mu m$, $\alpha = 0.059$ and $N_{BEC} = 40000$

To determine the critical velocity I look at the slope close to the origin:

$$v_c = \lim_{k\to 0}\frac{\omega(k)}{k} \tag{4.15}$$

Here I used the relatively simple approach of only calculating the slope between the first two points of the dispersion relation. This means a loss of accuracy, but should still give a good picture of what range the velocity is in and how it scales with the different parameters. The results are shown in Figure 4.4 and are in the range of $10^7\,\mathrm{m\,s^{-1}}$

The linear behaviour close to the origin is promising, as it indicates superfluidic behaviour. The region in which the system exhibits this behaviour can be influenced by the experimental parameters, as shown in Figure 4.3. For the values feasible for experimental realization, the critical momentum is in the region of $10^6\mathrm{m}^{-1}$. Increasing the absorption, for example by adding dyes or nano-particles[**7**], or increasing the photon number leads to a higher k_{crit} while a narrower cavity also is of use. Another factor is the longitudinal mode number. A higher q also corresponds to a higher k_{crit}.

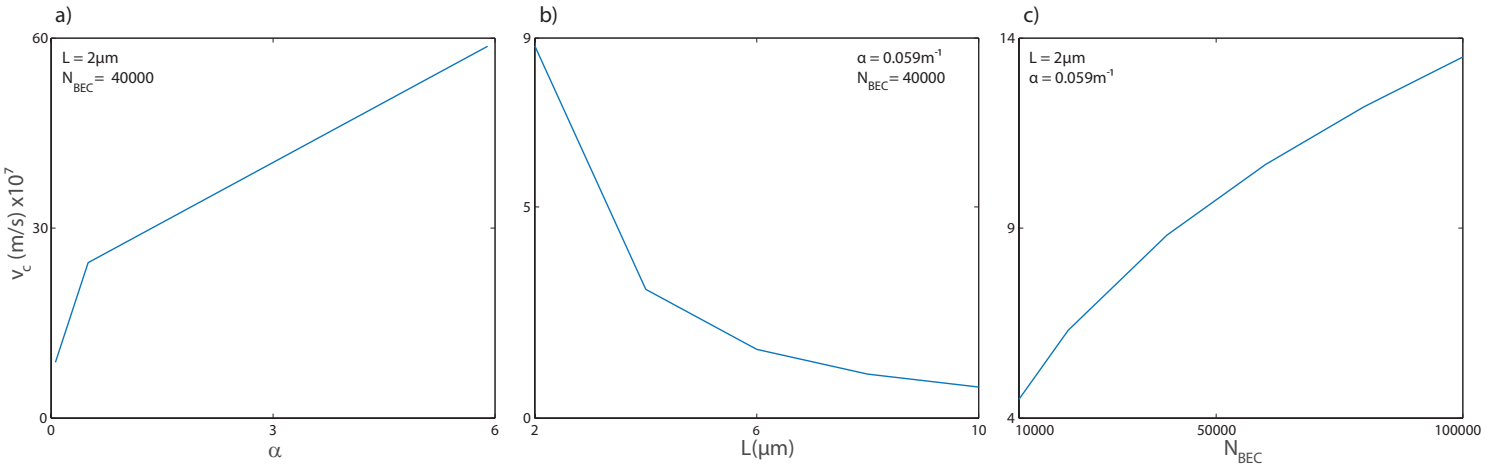

Figure 4.4: The critical velocity of the system depending on different parameters. As it was calculated via the slope of the dispersion relations previously found, there are only a few data points for each case. The general trend, however, is clearly visible, and follows that of k_{crit}: larger α and N_{BEC} increase the velocity, while L decreases it.

CHAPTER 5

Time Dependent Problem

To solve the time dependent case, the equation needs to be discretized in time and use interlacing time steps to calculate Ψ and T alternately. I decided to use the Crank-Nicholson method which is numerically stable[**10**]. To test my calculations, I solved the decoupled case (C and E being zero) analytically and compared the results. As it turned out the numerical solution showed some bad oscillations. A way to get rid of them is to add a damping term (called artificial viscosity in the literature[**11**]), which I implemented. After some tuning of the viscosity factor the numerical and analytical solution came to good a agreement.
To provide stability, he time steps have to be chosen carefully so that they fulfil the stability condition[**10**]:

$$|\frac{\alpha\Delta t}{\Delta x^2}| \leq 0.5 \tag{5.1}$$

with α being the coefficient in front of the Laplacian (in this case, it is B). This limits the computational capability, as I had to choose very small time steps in order to not lose accuracy in the z-direction, which in turn means that I had to go to a very large number of times steps to see the behaviour in time. This meant that due to a lack of computational power I was not able to compute the development from initial state to steady state.

5.1 Crank-Nicholson

The equations I need to solve are:

$$i\dot{\Psi} = A\Psi + B\nabla^2\Psi + CT\Psi \tag{5.2}$$

$$\dot{T} = D\nabla^2 T + E|\Psi|^2 \tag{5.3}$$

The Laplacian is calculated in a separate piece of code in the form of a matrix and thus not written explicitly here.

$$\dot{\Psi} = \frac{\Psi^{n+1} - \Psi^n}{\Delta t} = \frac{1}{2i}(A\Psi^{n+1} + B\nabla^2\Psi^{n+1} + CT^{n+\frac{1}{2}}\Psi^{n+1} + A\Psi^n + B\nabla^2\Psi^n + CT^{n+\frac{1}{2}}\Psi^n) \tag{5.4}$$

with n being the time step. This can be written as a function so that Ψ^{n+1} depends only on Ψ^n:

$$\Psi^{n+1} = \left(I - \frac{\Delta t}{2i}\left(A + B\nabla^2 + CT^{n+\frac{1}{2}}\right)\right)^{-1}\left(I + \frac{\Delta t}{2i}\left(A + B\nabla^2 + CT^{n+\frac{1}{2}}\right)\right)\Psi^n \tag{5.5}$$

with I being the identity matrix. The same principle holds true for $\dot{T}$. Ψ^{n+1} can then be used to obtain the next step in T, which is then plugged back into this equation, and so on. For stability, a viscosity factor $\nu\Delta t\nabla^2$ is included:

$$\Psi^{n+1} = \left(I - \frac{\Delta t}{2i}\left(A + B\nabla^2 + CT^{n+\frac{1}{2}}\right) + \nu\Delta t\nabla^2\right)^{-1}\left(I + \frac{\Delta t}{2i}\left(A + B\nabla^2 + CT^{n+\frac{1}{2}}\right) + \nu\Delta t\nabla^2\right)\Psi^n \tag{5.6}$$

ν is a numerical factor whose value was obtained through testing.

5.2 Excitation

To investigate how the steady state I found earlier might respond to small perturbations, one can write $\Psi(\vec{r},t) = (\Psi_{ss}(\vec{r}) + a(\vec{r},t))e^{-i\mu t}$ and $T(\vec{r},t) = (T_{ss}(\vec{r}) + \delta t(\vec{r},t))e^{-i\mu t}$. This can be plugged back into (5.3) and (5.2). After cancelling out the steady state solution and dropping the terms which are second order perturbation, this leads to a second set of equations:

$$\dot{a} = -i[(A-\mu) + CT_{ss} + B\nabla^2]a - iC\Psi_{ss}\delta t \tag{5.7}$$

$$\dot{\delta t} = E\Psi^*_{ss}a + E\Psi_{ss}a^* + D\nabla\delta t \tag{5.8}$$

This can also be written with the help of a matrix:

$$\frac{\partial}{\partial t}\begin{pmatrix} a \\ a^* \\ \delta t \end{pmatrix} = L\begin{pmatrix} a \\ a^* \\ \delta t \end{pmatrix} \tag{5.9}$$

with L given as

$$\begin{pmatrix} -i[(A-\mu) + CT_{ss} + B\nabla^2] & 0 & -iC\Psi_{ss} \\ 0 & i[(A-\mu) + CT_{ss} + B\nabla^2] & iC\Psi^*_{ss} \\ E\Psi^*_{ss} & E\Psi_{ss} & D\nabla^2 \end{pmatrix}$$

To solve these, I again used the Crank-Nicholson method with interlacing time steps. To account for energy that might be lost through the mirrors, a damping term β is added:

$$\dot{a} = [-i[(A-\mu) + CT_{ss} + B\nabla^2] - \beta]a - iC\Psi_{ss}\delta t \tag{5.10}$$

5.3 Eigenfrequencies

I used a time-harmonic excitation. One interesting thing is to find the eigenfrequency and observe if the amplitude of a becomes maximal if I excite at this frequency. To do so, wave function and temperature can be written as:

$$\Psi(\vec{r};t) = (\Psi_{ss}(\vec{r}) + u(\vec{r})e^{-i\omega t} + v^*(\vec{r})e^{i\omega t})e^{-i\mu t} \tag{5.11}$$

$$T(\vec{r};t) = T_{ss}(\vec{r}) + \delta t(\vec{r})e^{-i\omega t} + \delta t^*(\vec{r})e^{i\omega t} \tag{5.12}$$

Similarly to the case above this gives an eigenvalue problem:

$$\omega \begin{pmatrix} u(\vec{r}) \\ v(\vec{r}) \\ \delta t(\vec{r}) \end{pmatrix} = iL \begin{pmatrix} u(\vec{r}) \\ v(\vec{r}) \\ \delta t(\vec{r}) \end{pmatrix} \tag{5.13}$$

with L being the same as above.
For my calculations I used the steady state solution for $q = 1$ and $N = 0$. Due to the discretization of Ψ_{ss} and T_{ss} solving the eigenvalue problem gives a very large number of eigenvalues and eigenvectors, most of which are not physical. To find the proper eigenfrequency I looked at the corresponding vector for $u(\vec{r})$ to find those with the proper shape. As expected, there were certain frequencies matching different mode numbers, which are shown in Figure 5.1. It can be seen that the eigenfrequencies increase with the mode number q'. I also plotted the shape of $u(\vec{r})$ for two different eigenfrequencies. As in the steady state solution, they show the shape of the corresponding q'.

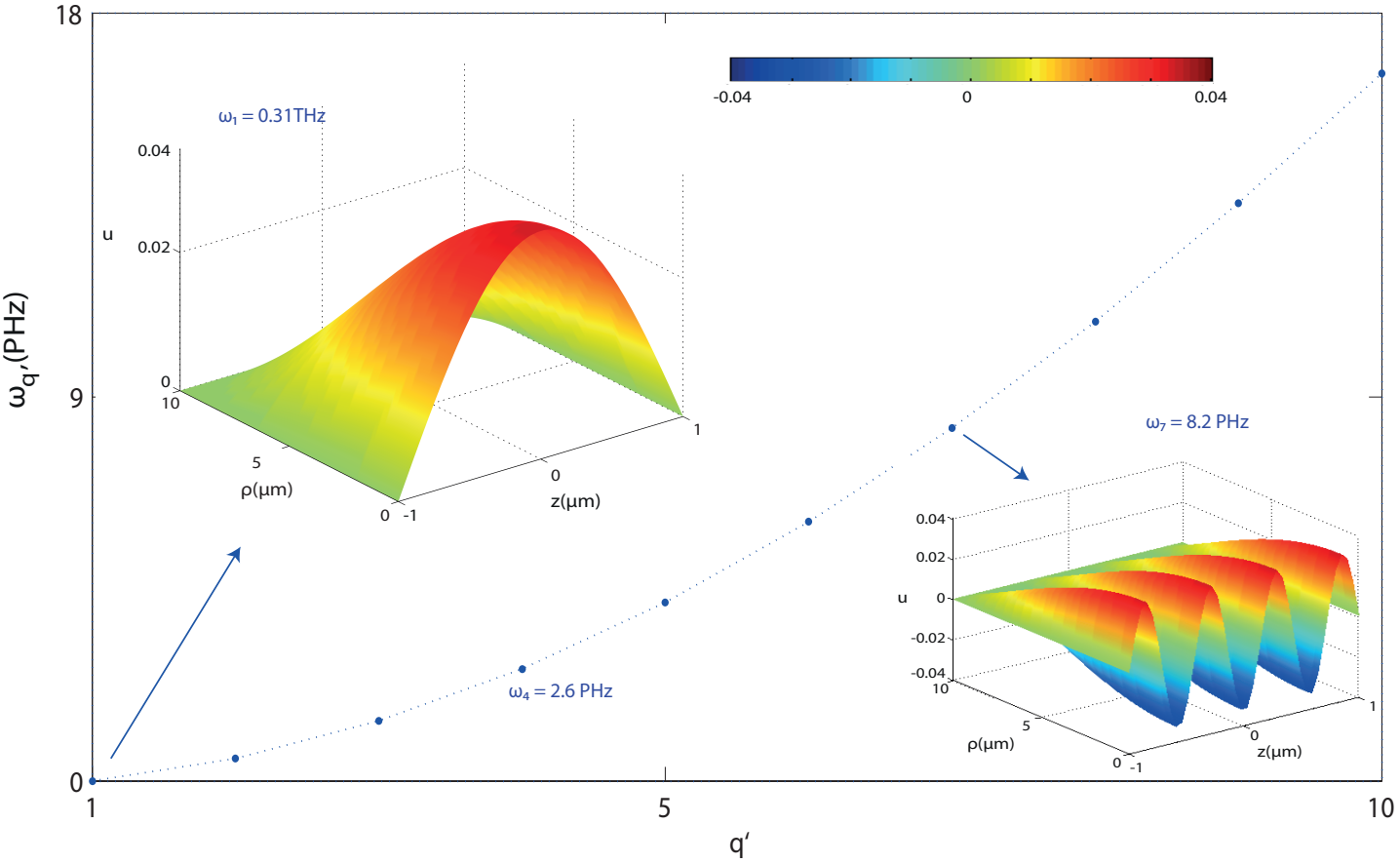

Figure 5.1: The eigenfrequencies I found for the system responding to different q'. Shown in a) and b) are $u(\vec{r})$ (in normalized units) for $q' = 1$ and $q' = 7$. As can be seen, it adopts the typical form also seen for the steady state. Note that this calculation was done for the steady state solution of $N = 0$ and $q = 1$. The shape here observed is merely a perturbation on top of that steady state form.

These were now used to harmonically excite the system. To implement this, at every time step I added

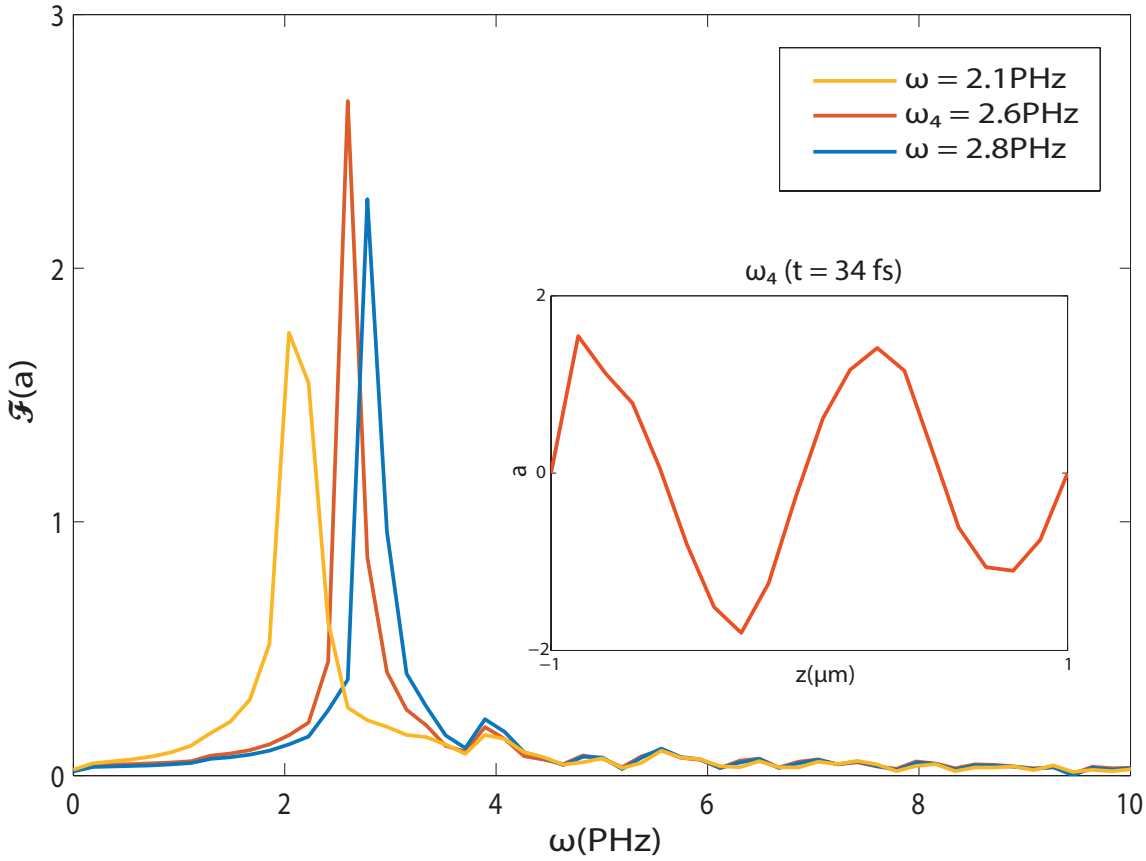

Figure 5.2: The Fourier transform of $a(t)$ (in normalized units) when perturbed with different frequencies ω. For the eigenfrequencies $\omega_4 = 2.63$ PHz one can observe the resonance of the system. The inlay shows $a(z)$ after 3000 time steps when perturbed at the eigenfrequency ω_4. The sinusoidal shape of $q = 4$ can clearly be observed. The original graph in the time domain can be seen in Figure A.8

the term $+i\frac{dn}{n_0}\frac{\omega}{2}\tau\sqrt{N_{BEC}}$ to $u(\vec{r})$ on the transversal plane closest to the mirror, which should mimic a perturbation on the mirror, i. e. shaking it or shooting a laser at it. Here, $\frac{dn}{n_0}$ is proportional to $cos(\omega_p t)$ with ω_p being the probing frequency. Computing the time development I found that the system picks up the excitation frequency very well. I found that exciting in a plane, which experimentally would mean moving the complete mirror, gave less convincing results than exciting in a spatially constraint manner, in this case with a narrow Gaussian form. If ω_p is chosen close to one of the previously found eigenfrequencies the amplitude rises, as the system is in resonance (see Figure 5.2). It also shows the form corresponding to the mode number of the excitation frequency.
While the eigenfrequencies found here are in the PHz region and thus not experimentally plausible, there is a possibility that they might be low enough if a steady state solution with a higher longitudinal mode number is considered, instead of the $q = 1$ case I used here.

CHAPTER 6

Conclusions and Outlook

To understand the system and investigate its properties, I first needed to solve the steady state solution, which was needed for further calculations
I managed to solve the steady state case reliably for several different cases. The response of the system to changes of experimental parameters was investigated. The time independent perturbation theory, while delivering slightly different values, gave a physical explanation for the observed behaviour with regard to absorption and photon number and confirmed the results.

The findings from the dispersion relation are very encouraging. While not sufficient proof, the Landau criterion offers a strong indication that superfluidity is possible. To clearly determine if the photon Bose Einstein condensate does exhibit superfluidity, other investigations are still needed. The region of interest for the critical momentum here lies at about $10^6\,\mathrm{m}^{-1}$. The linear behaviour can be influenced by the absorption, the photon number or the cavity length, as well as the longitudinal modes. To observe superfluidity, if it is possible, those parameters should be tuned correspondingly.

I did not manage to solve the time dependent case completely. However, early results were promising, and with greater computational power it should be possible to use the described method to reach the steady state. I found the eigenfrequencies for small perturbations on top of the steady state and was able to show that the system goes into resonance when being excited at these frequencies. While the values I found were impossible to realize, there is a chance that the eigenfrequencies might be low enough for higher mode numbers to experimentally observe the behaviour.

Bibliography

[1] A. Einstein, *Quantentheorie des einatomigen idealen Gases*, Sitzunsberichte der Preussischen Akademie der Wissenschaften, Berlin, Physikalisch-mathematische Klasse, 1924

[2] E. A. Cornell, C. E. Wieman et al, *Observation of Bose-Einstein Condensation in a Dilute Atomic Vapor*, Science **269**(1995)

[3] J. Klaers, J. Schmitt, F. Vewinger, and M. Weitz, *Bose-Einstein Condensation of Photons in an Optical Microcavity* Nature **468, 545** (2010)

[4] K. H. Bennemann, J. B. Ketterson, *Novel Superfluids Volume 1*, Oxford University Press, 2013

[5] University of Pittsburgh, 2008 C. Raman, M. Köhl, et al, *Evidence for a Critical Velocity in a Bose–Einstein Condensed Gas*, Phys. Rev. Lett.

[6] MATLAB version 8.3.0. Natick, Massachusetts: The MathWorks Inc., 2014

[7] Dr. Hadiseh Alaeian

[8] L. Landau, *Theory of the Superfluidity of Helium II*, Phys. Rev **60**, 1941

[9] V. B. Bobrov, S. A. Trigger, Prog. Theor. Exp. Phys.**2013**, 2013

[10] P. Johnson, *Stability for Parabolic Solvers*, 2008, retrieved from http://www.maths.manchester.ac.uk/~pjohnson/CFD/Lectures/parabolic_stability_handout.pdf

[11] A. Labovschii, *Mathematical Architecture for Models of Fluid Flow Phenomena*, Doctoral Dissertation, **83**(13), 1999

APPENDIX A

Appendix

Here, some additional information is shown. Table A.1 shows some results for the calculation of the singularity in the Green's function from chapter two, and compares value and computation time of Integration, Summation and the testing result of Mathematica.
Figures A.1 and A.2 show the influence of angular momentum and longitudinal mode number on the steady state solution, and Figure A.3 shows the steady state solution for the case of $N = 0$ and $q = 7$.
Figures A.4 to A.7 give some additional dispersion relations for different parameters, both for the non-local case as for the delayed one.
Figure A.8 shows the time development of $a(t)$ when excited with different perturbation frequencies. The Fourier transform of this graph is shown in 5.2.

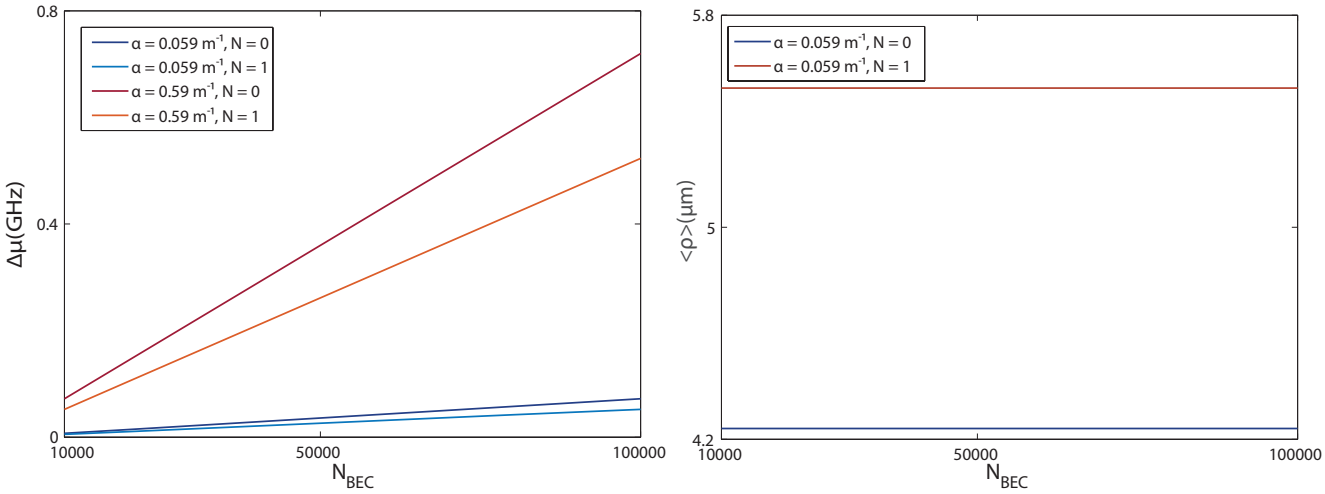

Figure A.1: $\Delta\mu$ in regard to N_{BEC} for different values of α and different angular momentum N in the case of $q = 1$.
So what?

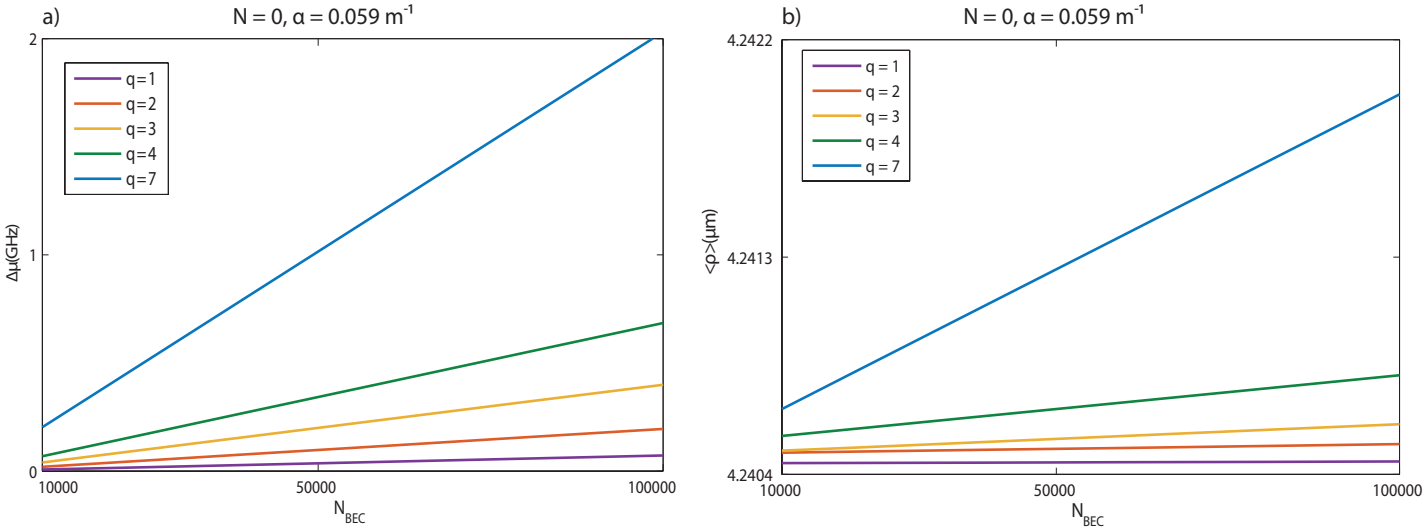

Figure A.2: $\Delta\mu$ and ρ depending on the photon number for different mode numbers q at $N = 0$ and $\alpha = 0.059\,\mathrm{m}^{-1}$. As expected, the non-locality increases with higher mode numbers.

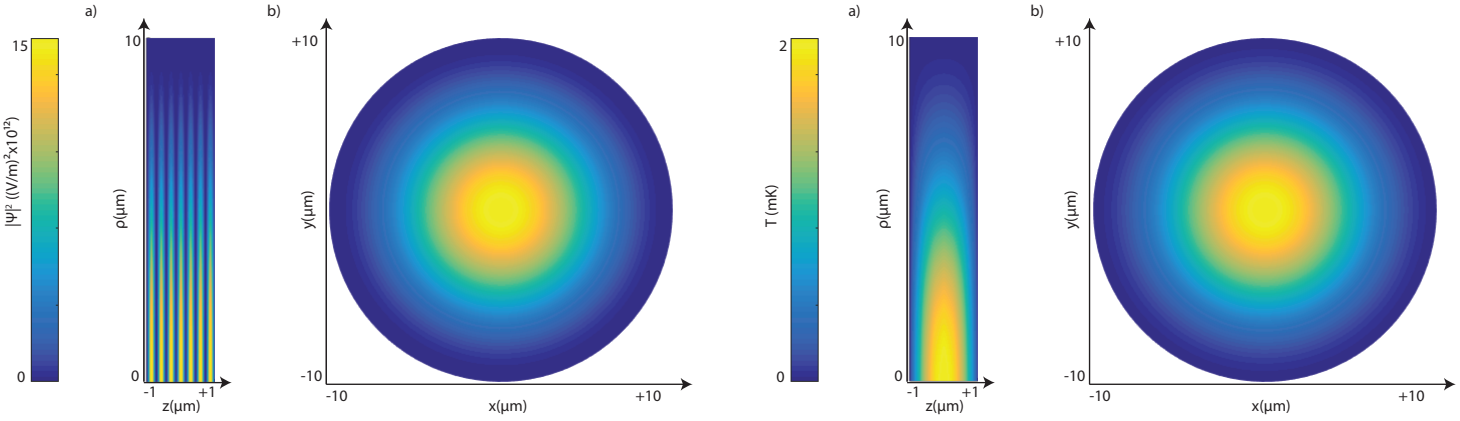

Figure A.3: This figure shows intensity of the wave function $|\Psi|^2$ (left) and the temperature T (right) both in the $\rho - z$-direction (a) and the $x - y$-plane (b) for $q = 7$ and no angular momentum. The other parameters were $N_{BEC} = 40000$ and $\alpha = 0.059\,\mathrm{m}^{-1}$

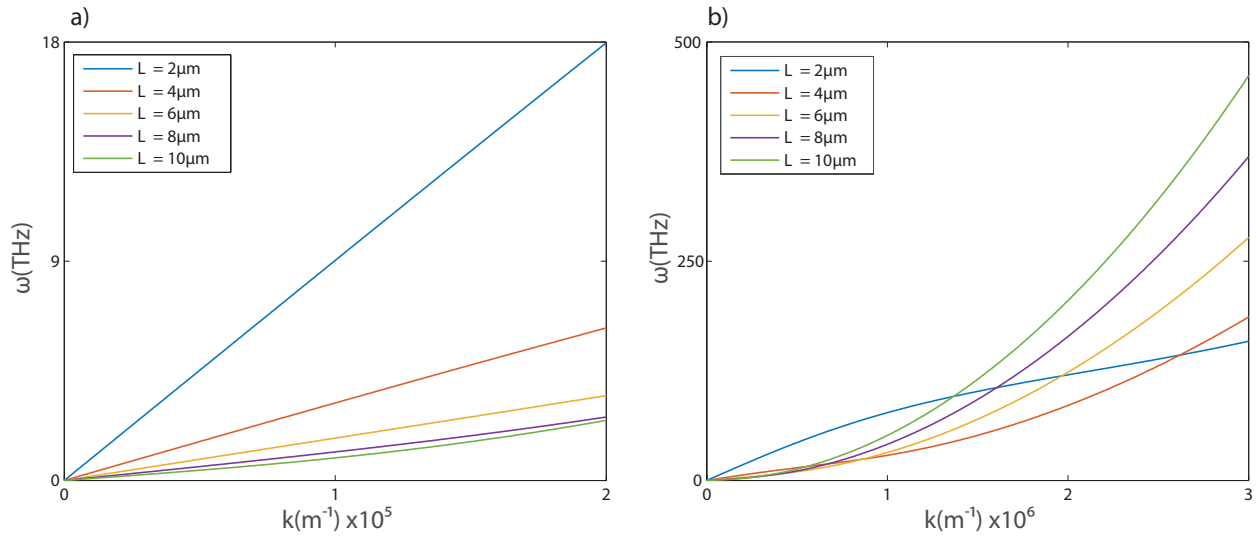

Figure A.4: The dispersion relation for the non-local case for different values of L. The photon number is $N_{BEC} = 40000$ and the absorption is $\alpha = 0.059\text{m}^{-1}$. The left figure a) shows the low-momentum part with the linear behaviour, while b) is more zoomed out, showing the change towards quadratic, free-particle behaviour.

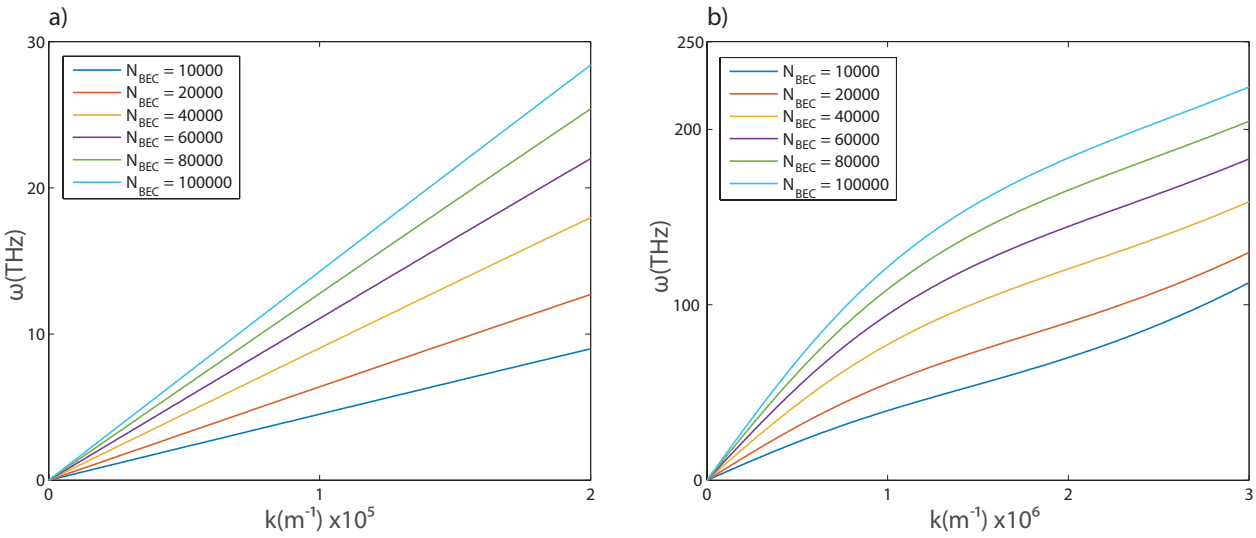

Figure A.5: The dispersion relation for the non-local case for different values of N_{BEC}. The length of the cavity is $L = 2\,\mu\text{m}$ and the absorption is $\alpha = 0.059\text{m}^{-1}$. N_{BEC} was varied between 10^4 and 10^5. The left figure a) shows the low-momentum part with the linear behaviour, while b) is more zoomed out, showing the change towards quadratic, free-particle behaviour.

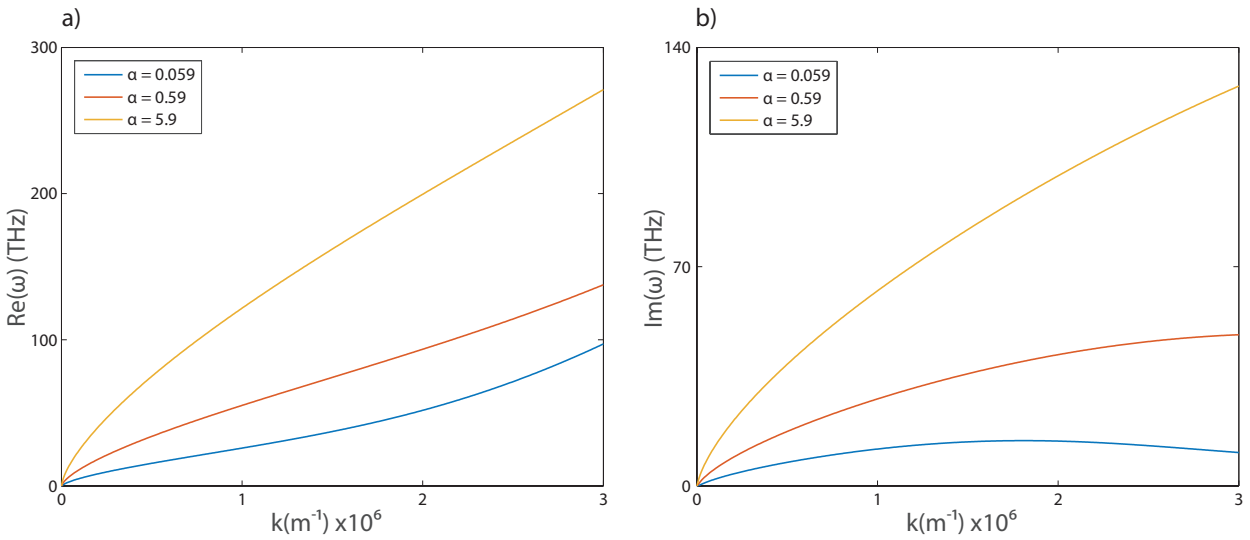

Figure A.6: The dispersion relation for the delayed case for different values of α. The length of the cavity is $L = 2\,\mu\text{m}$ and the number of photons is $N_{BEC} = 40000$. The left figure a) shows the real part of the frequency, while b) shows the imaginary part, i.e. the losses.

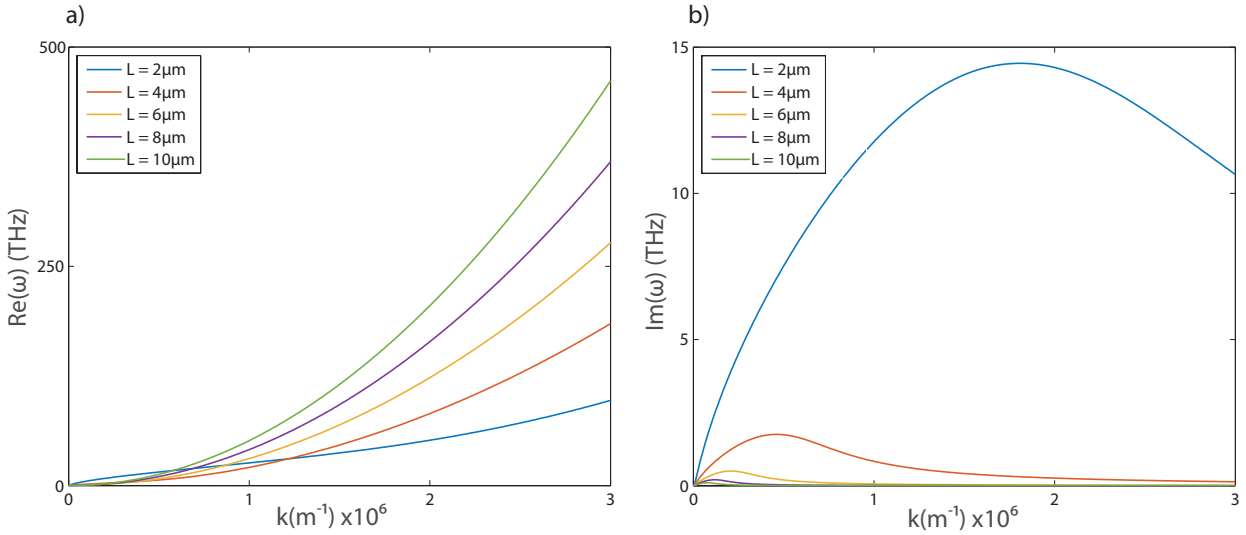

Figure A.7: The dispersion relation for the delayed case for different values of L. The photon number is $N_{BEC} = 40000$ and the absorption is $\alpha = 0.059\text{m}^{-1}$. The left figure a) shows the real part of the frequency, while b) shows the imaginary part, i.e. the losses.

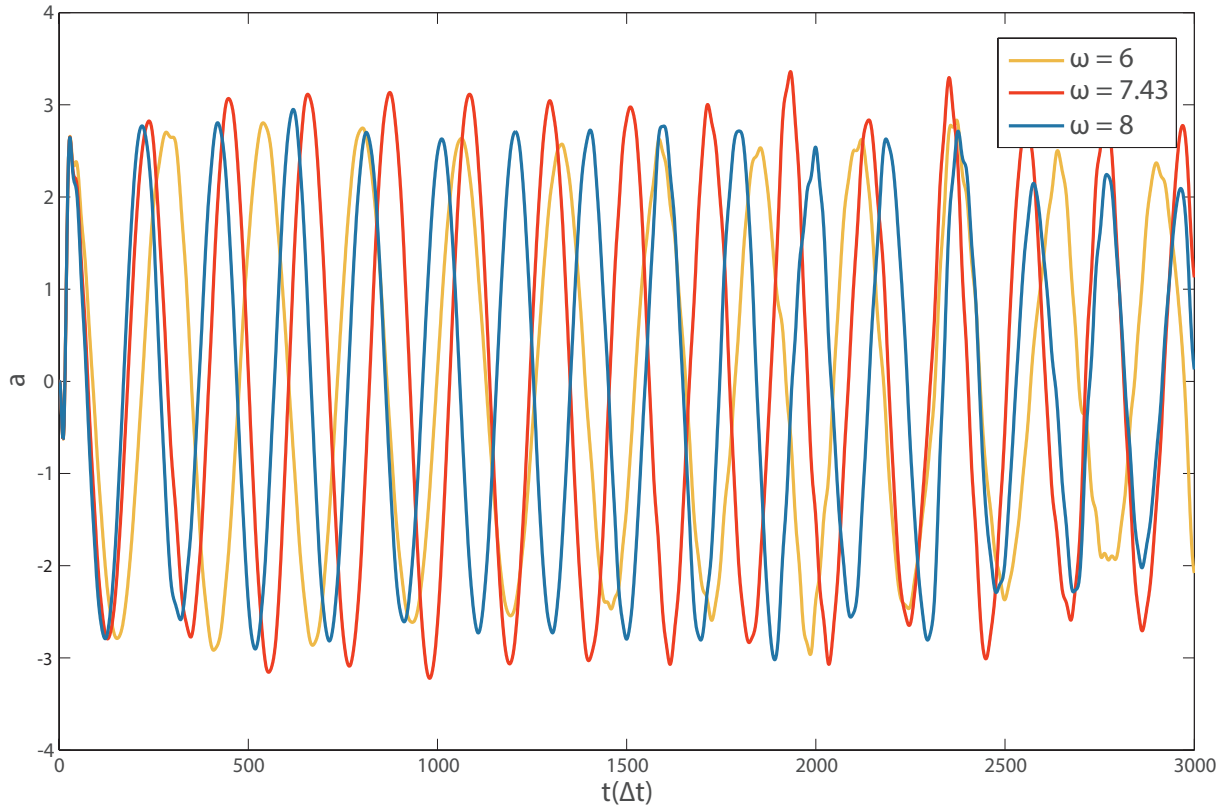

Figure A.8: $a(t)$ for different perturbing frequences ω. $\omega = 7.43$ here is the eigenfrequency for $q = 4$. One can see that the system is in resonance, as the amplitude is higher than for the other two cases. Note that these units are normalized. The frequency in real units is $\omega_{q=4} = 2.6\,\text{PHz}$. Δt corresponds to $0.004\tau = 0.01128\,\text{fs}$, meaning that the whole time span is about 34 fs.

Table A.1: Comparing value and computation time of The quad function in Matlab and the summation for different values of $\vec{\rho} = \vec{\rho'}$, represented by k_I and k_T. The data is not complete, but should suffice to see that while it takes very long, quad is in agreement with the results Mathematica gives. The summation however is not usable in this form

$k_I = k_T$	quad	time/s	Sum	time/s	Mathematica
16	-0.0300	5.409	-0.2292	0.007	-0.0299856
17	-0.0296	10.721	-0.292	0.021	-0.0296385
18	-0.0294	8.657	-0.3549	0.028	-0.0294122
19	-0.0294	10.063	-0.3955	0.027	-0.0293610
20	-0.0293	10.780	-0.4294	0.025	-0.0293414
21	-0.0293		-0.4586	0.028	-0.0293318
22	-0.0293		-0.4845	0.027	-0.0293264
23	-0.0293		-0.5292	0.028	-0.0293207
24	-0.0293		-0.5292	0.028	-0.0293207
25	-0.0293	12.957	-0.5489	0.024	-0.0293191
26	-0.0293		-0.5672	0.028	-0.0293180
27	-0.0293		-0.5843	0.027	-0.0293171
28	-0.0293		-0.6005	0.029	-0.0293165
29	-0.0293		-0.6157	0.028	-0.0293159
30	-0.0293	13.890	-0.6303	0.028	-0.0293155
31	-0.0387	5.610	-0.2407	0.007	-0.0387015
32	-0.0384		-0.3038	0.023	-0.0383940
33	-0.0380		-0.3489	0.028	-0.0379810
34	-0.0379				-0.0378885
35	-0.0379				-0.0378534
36	-0.0378				-0.0378361
37	-0.0378				-0.0378263
38	-0.0378				-0.0378203
39	-0.0378	13.421			-0.0378162
40	-0.0378	13.627			-0.0378134
41	-0.0378	13.764			-0.0378114
42	-0.0378	14.079			-0.0378098
43	-0.0378	14.792			-0.0378086
44	-0.0378	14.666			-0.0378078
45	-0.0378	14.792			-0.0378070
46	-0.0300	11.540			-0.0299856
47	-0.0296	25.956			-0.0296385
48	-0.0294	18.157			-0.0294122
49	-0.0294	21.195			-0.029361
50	-0.0293	21.446			-0.0293415
51	-0.0293	21.538			-0.0293319
52	-0.0293	24.443			-0.0293265
53	-0.0293	24.058			-0.0293231
54	-0.0293	23.271			-0.0293208
55	-0.0293	24.469			-0.0293193
56	-0.0293	24.678			-0.0293181
57	-0.0293	24.961			-0.0293173
58	-0.0293	26.584			-0.0293166
59	-0.0293	27.336			-0.0293161
60	-0.0293	26.085			-0.0293157

Acknowledgements

I would like to thank Prof Weitz for the opportunity to write my thesis in his work group. I would also like to thank Dr. Frank Vewinger for co-correcting this work. A very big thank also goes to Hadiseh, who helped me a great deal over the whole course of my work and taught me a lot about how to write a scientific thesis.